E. Sommer and D. Aurich†*

On the Effect of Constraint on Ductile Fracture

REFERENCE Sommer, E. and Aurich, D., **On the effect of constraint on ductile fracture**, *Defect Assessment in Components – Fundamentals and Applications*, ESIS/EGF9 (Edited by J. G. Blauel and K.-H. Schwalbe) 1991, Mechanical Engineering Publications, London, pp. 141–174.

ABSTRACT According to the principles of fracture mechanics it is expected that at any given position of a crack front, fracture should initiate and extend where the locally released energy exceeds the fracture resistance of the material. Therefore, for a precise prediction of crack growth characteristics, at least the distribution of the loading parameters such as the stress intensity factor K, the strain energy release rate G in the elastic, or the J integral in the elastic–plastic regime along the contour of the crack have to be known, as well as the distribution of the fracture resistance J_R. In cases where these parameters show a pronounced variation along the crack front the local consideration usually is replaced by a more integral one. For the sake of simplicity the fracture resistance is very often assumed to be constant along the contour. The more plastic deformation at the crack tip occurs, the more doubtful this assumption becomes. However, direct methods for determining the variation of the fracture resistance along crack contours are not available, therefore, sophisticated procedures have to be found. Since it is known that the local constraint greatly affects the fracture resistance these two quantities will be discussed. The constraint is considered to be the restraint of plastic deformation due to the specimen geometry and type of loading. The term 'constraint' is difficult to define in a quantitative manner. For ductile fracture the parameter σ_m/σ_v has successfully been applied to characterize the local constraint at the crack tip, where σ_m is the mean stress and, σ_v the equivalent stress. It will be demonstrated that the experimentally-found crack growth behaviour of surface cracks more precisely can be predicted. Furthermore, the reported results are considered as one of the necessary links in the chain of transferability of test results from specimens to components.

Notation

a	Crack length
Δa	Crack growth
c	Maximum depth of a semi-elliptical surface crack
d_n	Proportionality factor of the δ-J-correlation
f	Volume fraction of voids
r, s, θ	Plane system of coordinates of a crack; three-dimensional coordinate system at the tip of a surface crack
r_i	Inner radius of a pressure vessel
t	Wall thickness
v	Displacement in y-direction
x, y, z	Three-dimensional system of coordinates of a crack, x is the potential crack growth direction, z is the direction parallel to the crack front
B	Specimen thickness

* Fraunhofer-Institut für Werkstoffmechanik, Freiburg, FRG.
† Metals and Structures of Metals Division, Bundesanstalt für Materialforschung, Berlin, FRG.

F	Force, load
J	J-integral
J_i	Physical initiation toughness
J_i^{mean}	Mean J_i of different specimen sizes tested at different temperatures
J_{Ic}^{ASTM}	Technical initiation toughness according to ASTM E 813-81
J_{Ic}^{Loss}	Technical initiation toughness according to Loss *et al.*
J_R	Crack resistance
$K_{\sigma p}$	Plastic stress concentration factor
$N = 1/n$	Work hardening exponent
R	Notch root radius
R_{eL}	Lower yield point
$R_{p0.2}$	0.2 percent proof strength
S	Arc length of SCT
T	Temperature
W	Specimen width
α	Work hardening factor
δ_t	Crack tip opening displacement
ε_v	Equivalent stress
σ_m	Mean stress
$\sigma_{1,2,3}$	Principal stresses
σ_{xx}	Stress in ligament direction
σ_{yy}	Crack opening stress
θ	Angle describing the position along a semi-elliptical surface crack
$\varnothing$	Diameter

Indices

$^\circ$	Initial value
mean	Mean value, averaged in z-direction

Abbreviations

$\max_x$	Maximum of the subsequent quantity in x-direction
$\max_{x,\Phi}$	Maximum of the subsequent quantity in x- and Φ-direction

Specimen geometries

CCT	Centre cracked tension specimen
CNT	Centre notched tension specimen
CT	Compact tension specimen; the number behind characterizes the specimen thickness
DECT	Double edge cracked tension specimen
Inst.	Instable; instability
MSU	Multiple specimen unloading
SCT	Surface crack tension specimen
SECT	Single edge cracked tension specimen
SSPUC	Single specimen partial unloading compliance
TPB	Three point bending specimen

Criteria for ductile fracture

Disastrous accidents in the thirties and forties of this century caused by cleavage fracture forced material scientists to take better precautions. New steels with lower ductile-cleavage transition temperature, new welding procedures as well as improved standards and codes have been developed. As a consequence of this work, damage due to cleavage fracture has become very exceptional. By means of linear elastic fracture mechanics margins of safety, even quantitatively, can be determined.

Although such tools allow the selection of materials and the establishment of regulations in order to ensure a reliable operation of components above ductile-cleavage transition temperature, it should be kept in mind that the ductility of many engineering materials is not a general guarantee for the avoidance of ductile failure under all loading situations. As a consequence, more attention had to be paid to the field of ductile fracture in order to develop appropriate fracture criteria which allow the determination of data characteristic for material, fracture properties, and useful for the assessment of components.

Under the conditions of small-scale yielding, ductile fracture can be treated by the criteria established on the base of linear elastic fracture mechanics. However, in practice these criteria mainly apply to materials of low ductility. Therefore, for the assessment of rather tough materials there was a strong desire to develop criteria for ductile fracture of similar simplicity.

Crack tip opening displacement δ_t as well as J-integral or other path-independent integrals are considered to be very serious candidates for such types of criteria. J and δ_t are interrelated by the relationship

$$\delta_t = d_n J/R_{eL} \tag{1}$$

The conditions and limitations supposed for the existence of an HRR-field and thus for J-controlled fracture,

- proportional loading,
- small crack tip deformation, and
- plane strain or plane stress conditions,

should apply to the crack tip opening displacement criterion, too. Therefore, further consideration of constraint effects are restricted essentially to J.

The parameter J, originally defined as a path-independent line integral in a plane containing a crack, also gives evidence of the stress and strain concentration in the near field of the crack tip, as well as of the deformation energy release rate. In cases where the usual requirements are met, J turns out to be a useful single parametric criterion for the assessment of ductile fracture. However, more detailed investigations show that even plane specimens have to be considered as three-dimensional bodies with respect to ductile fracture.

Whereas the initiation of cleavage fracture can be traced back to a single nucleus, the initiation and growth of ductile fracture takes place in process zones of finite size along the whole crack contour. In order to ensure uniform conditions for initiation along the crack contour, special precautions as side-grooving the specimen are needed.

This raises the general question of applicability of J to three-dimensional crack problems in different types of specimens as well as in components. This question is strongly connected to the problem of constraint. In the field of material science and fracture mechanics, the term constraint is often used in a qualitative manner since a precise and complete definition is difficult to provide. When constraint is understood as the restraint of deformation, it depends on the boundary of a specimen or component, the acting forces, and the properties of the material used. It is extremely affected by gradients of stresses or strains due to notches and cracks in specimens or components. This again means that the resulting global and local stress states which, in general, only implicitly can be accounted for, have a pronounced influence on the fracture process.

Quantitatively, the importance of constraint for failure has been recognized by many authors since the thirties of this century **(1)–(11)**. The cited publications may be considered as examples only, because a very large number of papers have been published in this field. Compiling all this knowledge, one obtains roughly the following state of the art in this area: constraint in notched or pre-cracked specimens or components is caused by geometrical discontinuities and the type of loading. One has to distinguish between global and local constraint which influence the stress state at the crack tip. The influence of geometry on constraint may be separated in two main parts: in-plane and out-of-plane constraint. Based on plane specimens 'in-plane' means acting of constraint in the plane of the specimen, i.e. in x-y-plane, and 'out-of-plane' means acting of constraint in planes perpendicular to the x-y-plane, i.e. in x-z- and y-z-plane. In analogy, these definitions may be extended to components. The in-plane constraint is governed by the location of the crack in the x-y-plane, e.g. in a single edge (SECT), double edge (DECT), or centre cracked (CCT) tension specimen, the crack depth and the type of loading, e.g. tension or bending. The high local in-plane constraint, e.g. in a pre-cracked bending specimen, is caused by the immobility of the crack tip and the opposite surface resulting from the global rotation of the two halves of the specimen around the 'rigid' pivot. The out-of-plane constraint is mainly influenced by the thickness of the specimen or component. The higher the constraint the more plastic deformation at the crack tip will be restrained. Experimentally it can be observed that constraint affects the slope of crack resistance curves.

Therefore, it is felt that there is a need for a quantitative explanation of the effect of constraint and local stress states on ductile fracture. Investigations of this kind will provide additional parameters for a precise J-based assessment of ductile fracture processes.

A first motivation for such investigations results from some experimental observations which are not completely in accordance with the application of J as a single parametric fracture criterion.

Experimental observations

For engineering purposes standardized methods which allow for a reliable characterization and assessment of initiation and growth processes of ductile fracture are needed. The parameter J has been successfully applied for obtaining reproducible material data describing the onset and stable growth of fracture in plane specimens by confining the range of variation of the involved geometry and loading parameters. This is the well known procedure e.g. of ASTM E 813-87 **(12)**. But even when such restricting evaluation procedures are applied, a pronounced variation in the resulting data cannot be avoided.

Fracture initiation

When fracture initiation is considered to be a local event and is described by a single parameter as J only, comparable situations regarding the microstructural properties as well as the mechanical and the geometrical conditions in the corresponding process zones of different types of specimens should prevail. As a consequence, the more localized the initiation process will be, and the more different the types of investigated specimens are, the more uncertainty of the experimentally obtained data must be expected and will appear in the statistical scatter. In addition, it has to be accounted for that even in plane specimens (non sidegrooved) the loading parameter J may vary along the crack contour while the experimental determination of J from force-displacement records leads to average values $J_{\text{mean}} = B^{-1} \int J(z)\,\mathrm{d}z$ (B = thickness).

Neglecting for the first instance these detailed considerations the initiation of fracture can be characterized according to several evaluation procedures. In Fig. 1 toughness values for the reactor pressure vessel steel 20 MnMoNi 55 are compared which have been determined **(13)** corresponding to the following definitions:

- $(J_{\text{Ic}})^{\text{ASTM}}$ technical initiation toughness-evaluated from a linear fit to the J-resistance curve according to ASTM E 813-82 **(12)**,
- $(J_{\text{Ic}})^{\text{Loss}}$ technical initiation toughness-evaluated from a power law fit proposed by Loss *et al.* **(14)** and
- J_{i} physical initiation toughness-estimated as the first point of deviation of the J-resistance curve from the formal blunting line.

The technical 'initiation' toughness does not correspond to the real onset of fracture but to a finite amount of stable crack growth of approximately 0.3 or 0.4 mm and is, therefore, higher than the physical initiation toughness. In addition, temperature trends are observed at about 200°C.

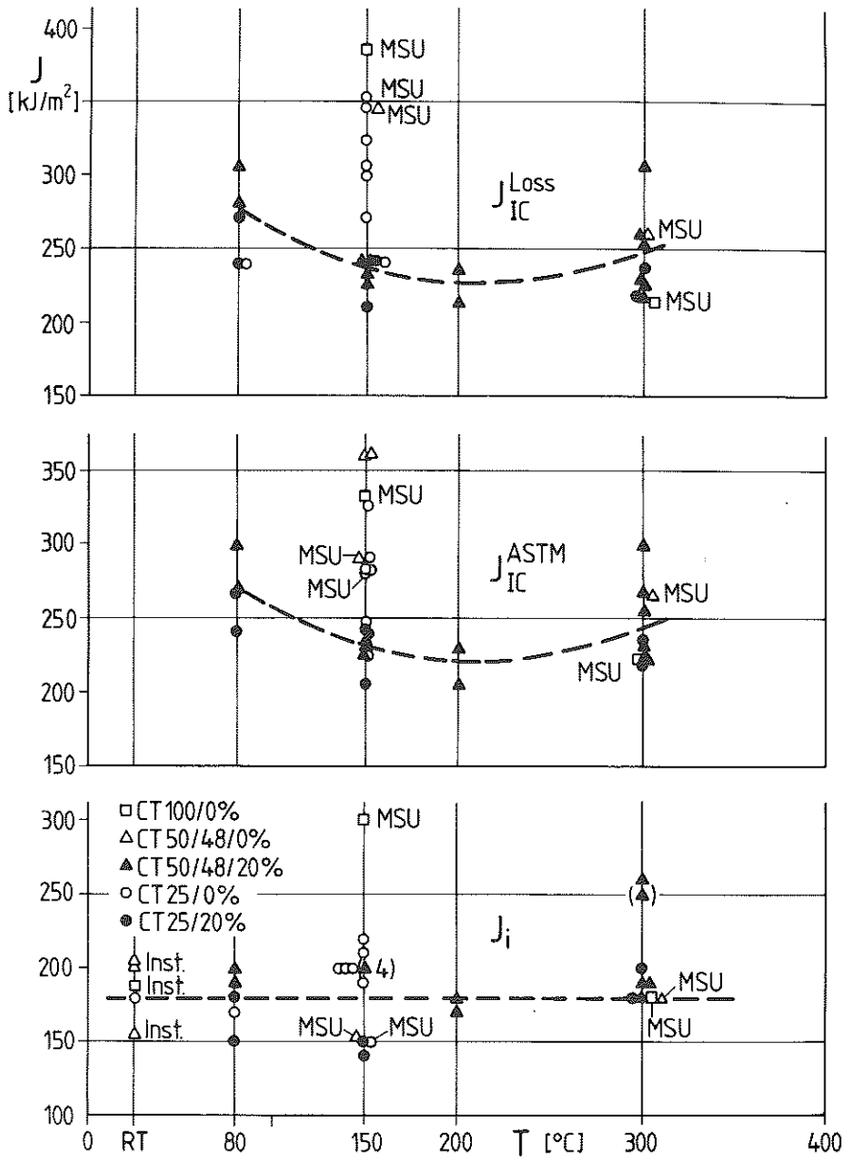

Fig 1 Initiation toughness as a function of temperature; pressure vessel steel 20 MnMoNi 55 (13)

The physical toughness values J_i can be determined only with considerable uncertainty. Although within a pronounced scatterband these J_i-values seem to be independent of geometry parameters – at least in the range of variation of CT 25–CT 100 with and without sidegrooving – and of temperatures – in the range of variation of room temperature to 300 degrees C. As a mean value results $(J_i)^{mean} = 180$ N/mm.

These findings seem to be in contradiction to the following considerations. As mentioned above, J_i-values have to be interpreted as mean values since they are averaged over the thickness of the plane specimen used for determining the complete J-resistance curve. Therefore, it should be expected – when fracture initiation is really a local event – that in specimens with and without sidegrooving different J_i-values will result since the J-distribution and thus the mean values $(J_i)_{mean}$ are different as well – as can be seen from Fig. 8 in the next section where the numerically calculated J-distributions are plotted. This trend can be observed in Figs 2 and 3 where $(J_i)_{mean}$ (20 percent s.g.) $\approx 200 \pm 20$ N/mm and $(J_i)_{mean}$ (0 percent s.g.) $\approx 160 \pm 20$ N/mm which in both cases corresponds to a *highest* local value of about $J_i \approx 190$ N/mm. In general, the experimental error of 10–20 percent does not allow to resolve such effects.

Stable crack growth in plane specimens

Whereas the pronounced influence of the sidegrooving on the slope of J-resistance curves already can be demonstrated by Fig. 2, the following examples will cover a wider range of variation of the specimen geometry and implicitly the variation of the local constraint situations. In Fig. 4 a variety of J_R-curves obtained for the reactor pressure vessel steel 20 MnMoNi 55 at 80°C in different CT-specimens **(13)**. The range of variation investigated is:

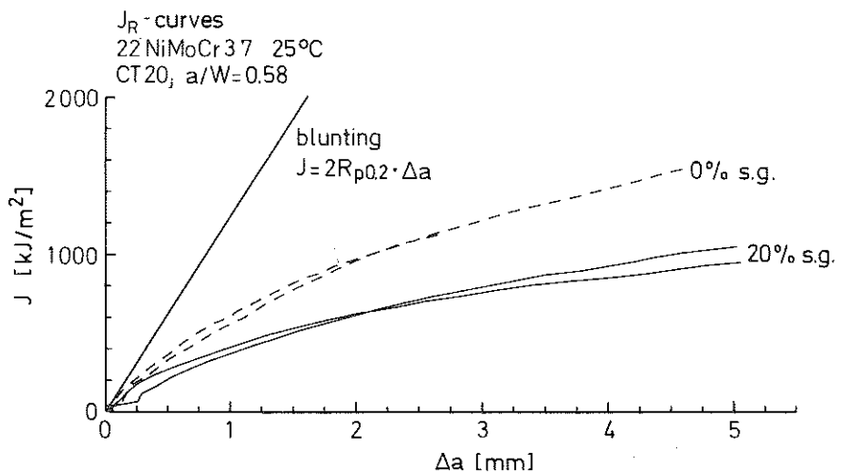

Fig 2 J_R-curves of CT 20 specimens 0 percent and 20 percent side grooved; reactor pressure vessel steel 22 NiMoCr 37 (29)

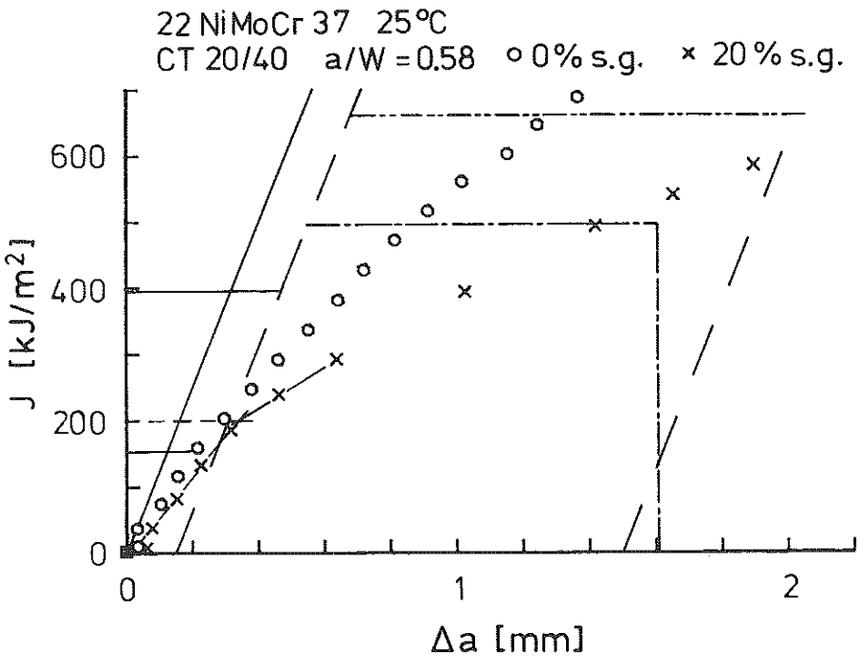

Fig 3 Details of Fig. 2; two curves selected from four in order to demonstrate the difference in the onset of stable crack growth for specimens 0 percent and 20 percent side grooved (29)

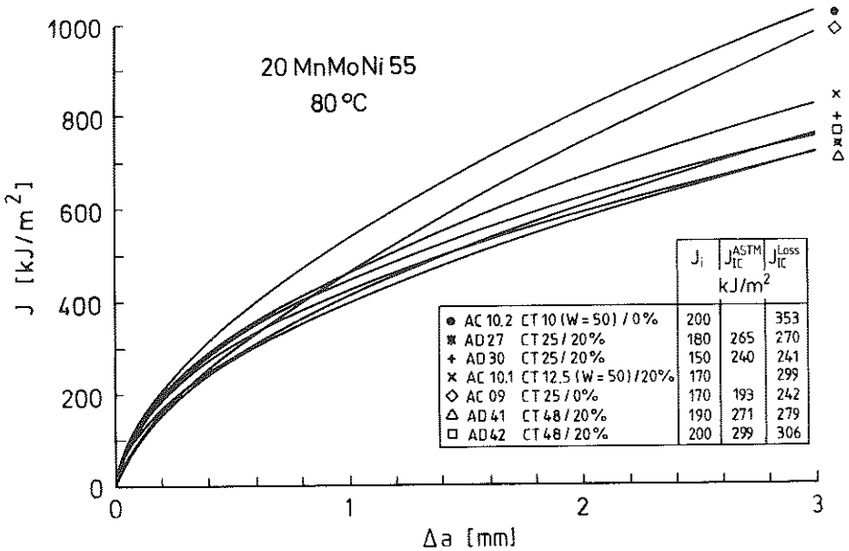

Fig 4 J_R-curves and critical J_I-values obtained from different CT-specimens at 80°C with the partial unloading technique for the reactor pressure vessel steel 20 MnMoNi 55 (13)

CT 10–CT 48 (7 specimens) with (20 percent) and without (0 percent) side-grooving; the steepest slope is obtained for the two specimens CT 10 (0 percent) and CT 25 (0 percent); the lowest slope for four curves within the same scatterband of CT 48 (20 percent) and CT 25 (20 percent). The slope of the CT 12,5 (20 percent) specimen is also as low as for the 20 percent side-grooved specimens CT 25 and CT 48 which means that 20 percent side-grooving of small specimens ($B < 25$ mm) has a stronger effect on the slope than doubling the specimen thickness.

In Fig. 5 J_R-curves obtained for several types of plane specimens and for a vessel ($\varnothing = 1500$ mm, $t = 40$ mm) with axial through cracks ($2a = 104$–450 mm) are compared **(15)**. The material investigated is the steel StE 460 ($R_{eL} =$ 490 MPa). The slope of the resistance curves found for the CT-specimens is considerably lower than that observed for CCT-specimens. However, the slope of the curves for the axial cracks in the vessel test is almost as low as that of the CT-specimens which demonstrates that an assessment of this configuration on the basis of CCT-results would have been completely misleading. In order to provide reliable test data for assessment procedures, investigations of even more complex crack configurations as surface cracks in plates and vessels are needed.

Behaviour of surface cracks

For characterizing the growth behaviour of surface cracks as a typical example, the following tests may stand **(16)** which concentrate on the investigation of the extension of a crack in a pressure vessel of the high strength steel

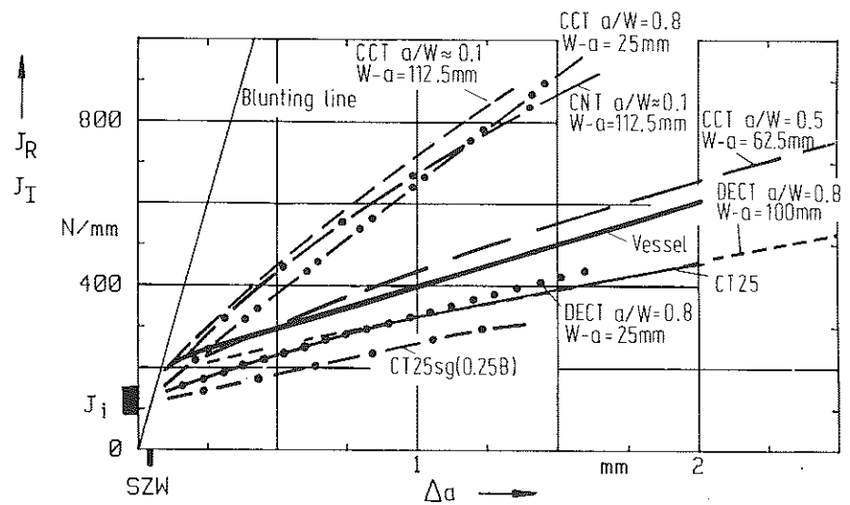

Fig 5 J_R-curves for axial-through-the-thickness cracks in a cylindrical vessel ($\varnothing = 1.5$ m) and three different types of specimens; steel StE 460 at 25°C (15)

($\varnothing$ = 1.5 m); steel StE 460 at 25 °C

20 MnMoNi 55 (= A 533 B, R_{eL} = 460 MPa). The initial flaw located in the cylindrical part of the pressure vessel ($\varnothing$ = 1500 mm, t = 40 mm) in axial direction was extended alternately by fatigue and stable crack growth at room temperature. The resulting fracture surfaces are shown in Fig. 23. Very similar results have been obtained with the steel StE 460 **(17)**. More detailed investigations, as discussed below, show

- that the crack contours after stable crack growth are not semi-elliptically-shaped ('canoeing effect') because the maximum of local crack extension is not found in the centre (angle $\Phi = 0$ degrees), but in a range, 60 degrees $< \Phi <$ 80 degrees,
- that the maximum amount of stable crack growth does not coincide with the maximum of the loading parameter J numerically calculated along the crack contour and
- that the slope of J_R-curves locally constructed at several points along the crack contour differ considerably from that of a resistance curve from a sidegrooved CT 25 specimen – except in the range 60 degrees $< \Phi <$ 80 degrees – where the maximum crack growth occurs.

It can be concluded that phenomena of this kind cannot be explained without taking into account

- the local constraint situation along the crack contour and
- the micromechanical effects determining the initation and extension of cracks as will be discussed.

Numerical results

Constraint has manifold implications with respect to geometry, stresses and strains. For example, the above-mentioned large in-plane constraint in a CT-specimen causes the ligament to extend during the increase of the loading, whereas the relatively small in-plane constraint in a CCT-specimen results in reduction of ligament length **(18)** (Fig. 6). Similar implications are well known for the out-of-plane constraint comparing plane strain and plane stress conditions.

Local constraint

A further expression of constraint in analogy to the theory of plasticity of notches can be seen in Fig. 7 **(19)**. If the plastic stress concentration factor as measure of constraint is defined as

$$K_{\sigma p} = \max_x \left(\frac{\sigma_{yy}}{R_{eL}} \right) \tag{2}$$

one concludes from Fig. 7 that constraint in a CT-specimen is significantly higher than in a CCT-specimen.

At present, the understanding is that ductile fracture is governed by a loading parameter as J and a parameter as σ_m/σ_v indicating the effect of constraint on the local stress state near the crack tip in a more general manner than the plastic stress concentration factor **(20)–(26)**. The parameter σ_m/σ_v is given by

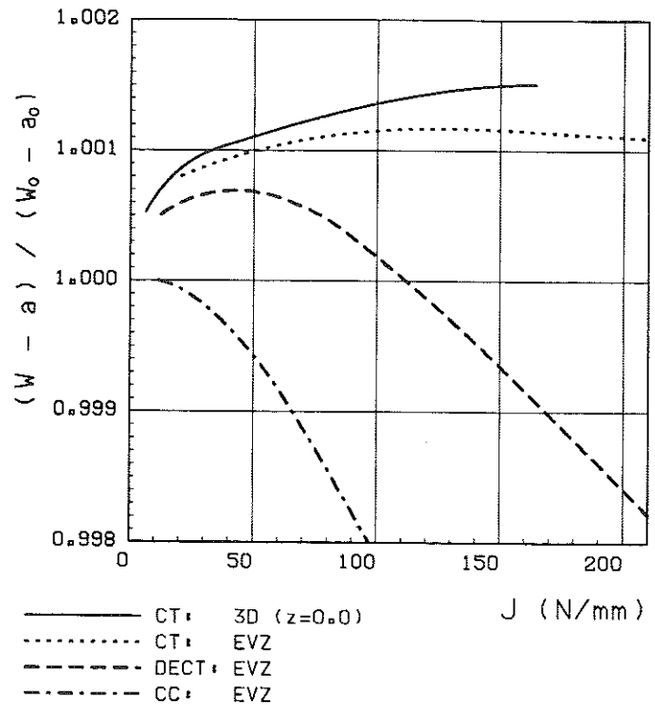

Fig 6 Variation of normalized ligament length $(W\text{-}a)/(W_0\text{-}a_0)$ with increasing J for CT- (3D and 2D plane strain), DECT- (2D plane strain) and CCT-specimen (2D plane strain) obtained by FEM (18); pressure vessel steel 20 MnMoNi 55

mean stress $\sigma_m = (\sigma_1 + \sigma_2 + \sigma_3)/3$ *and*

equivalent stress $\sigma_v = 2^{-1/2}[(\sigma_1 - \sigma_2)^2 + (\sigma_3 - \sigma_1)^2 + (\sigma_2 - \sigma_3)^2]^{1/2}$

The ratio σ_m/σ_v will be considered for a local volume element in the neighbourhood of a crack tip and depends on material properties, external load, and geometry as a function of all three coordinates r, θ, s.

For the interpretation of experimental results concerning initiation and stable growth of ductile fracture, therefore, not only the influence of the local variation of the loading parameter J along the contour but also the local variation of constraint has to be investigated. For mode I loading the constraint is highest in the plane $\theta = 0$. For this reason and for the sake of simplicity the following considerations will be based on the assumption that the constraint variation along the contour at $\theta = 0$ is most important for ductile

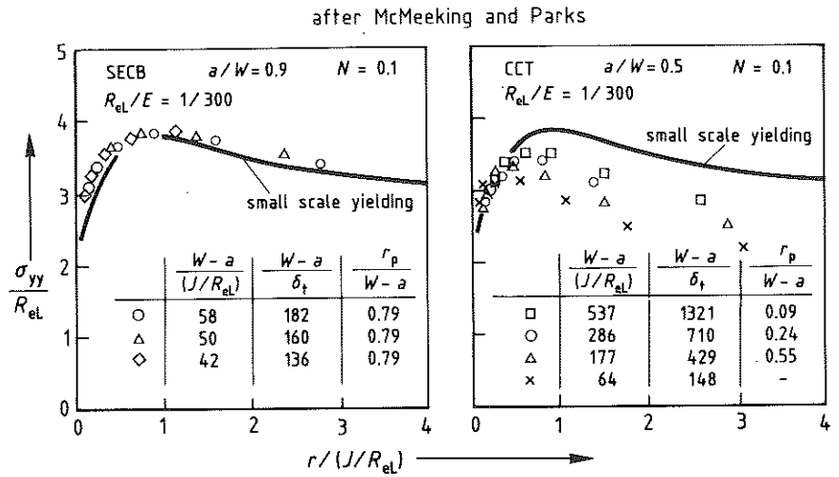

Fig 7 Normalised crack opening stress σ_{yy}/σ_0 versus normalised ligament $r/(J/\sigma_0)$ obtained by 2D-FEM: edge-cracked bend type specimen in comparison with a centre cracked panel; work hardening exponent $N = 0.1$ (19)
(a) edge-cracked bend type specimen, $a/W = 0.9$
(b) centre cracked panel, $a/W = 0.5$

fracture. Doing so, the influence of the size and geometry of various test specimens and components and the loading configuration on J and the parameter σ_m/σ_v can be analysed. Subsequently a series of characteristic specimens and pre-cracked components of interest from the engineering point of view will be investigated and compared.

Local constraint and non growing cracks

During the last decade the capability of the FE-method has been improved so remarkably that nearly every relevant information on stresses and strains can be obtained in the far tip field as well as in the near tip field of a crack. At present, most results are available for non-growing cracks.

When the local constraint is described by the ratio σ_m/σ_v and is calculated by FE-method the accuracy of results depends on the technique used for modelling the crack tip field, the type and mesh size of the elements **(27)(28)**. If, for instance, the updated Lagrangian option in a FE-program and fine mesh size are used, the function $\sigma_m/\sigma_v = f(r)$ shows a maximum at a definite distance of the crack tip. For the same material properties and the same J this maximum is mainly affected by effects related to the specimen geometry and type of loading **(18)(27)**. For scanning purposes some authors **(29)(30)** prefer a more integrating approach using coarse mesh size and MNLO-modelling for the calculation of $\sigma_m/\sigma_v = f(r, s, \Theta)$. MNLO (material non linear only) does not take into account geometric non-linearities.

The most commonly used specimen in fracture mechanics is the CT-specimen. In Fig. 8 the loading parameter J and the ratio σ_m/σ_v along the contour of a CT-specimen without side grooves are compared with those of a CT-specimen with 20 percent sidegrooving **(28)–(30)**. In the non-sidegrooved specimen the mean value J_{mean} as obtained normally from experiment is 20 percent lower than the maximum value and approximately the same is true for the ratio σ_m/σ_v. This result may match the experience that in non-sidegrooved specimens distinct tunnelling of the growing crack is observed. It

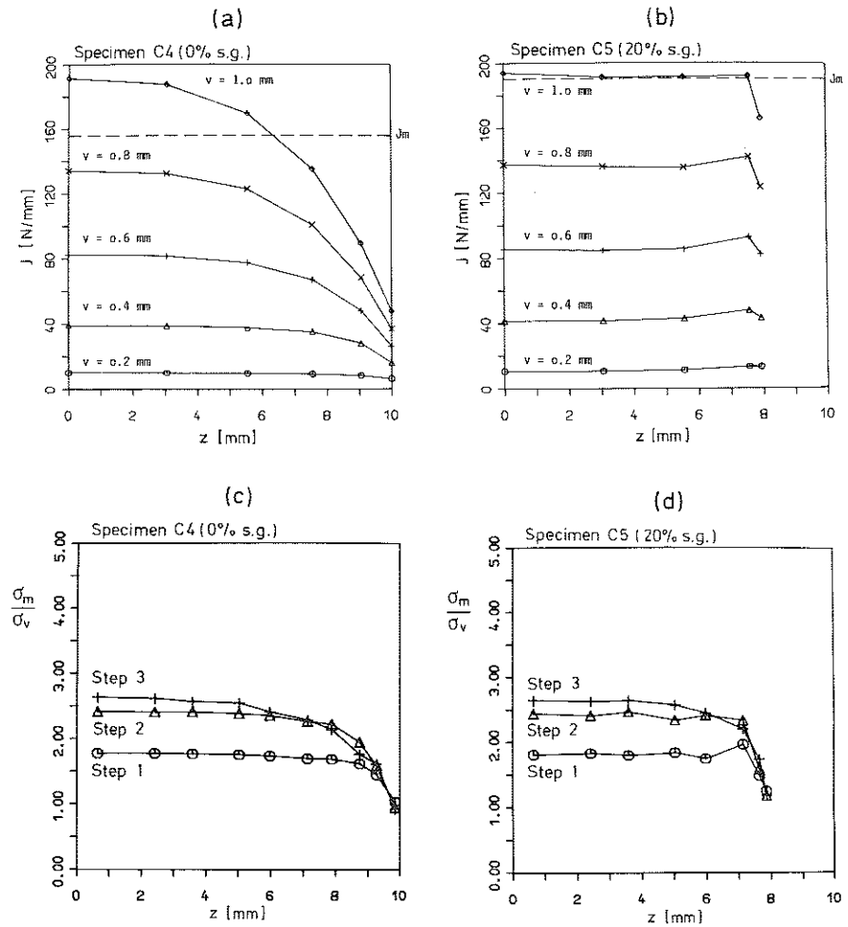

Fig 8 Variation of J-integral (v_i = steps in displacement) and of the ratio σ_m/σ_v along the crack front in direction z of a CT-specimen from centre to surface obtained by 3D-FEM (29)
(a) J of 0 percent sidegrooved specimen
(b) J of 20 percent sidegrooved specimen
(c) ratio σ_m/σ_v for $r = 0.2$ mm of 0 percent sidegrooved specimen
(d) ratio σ_m/σ_v for $r = 0.2$ mm of 20 percent sidegrooved specimen

will be demonstrated below that this phenomenon has an even more complex background. Fortunately, in these specimens the maximum of J coincides with that of the ratio σ_m/σ_v and the problem of gradients along the crack contour can be overcome completely by sidegrooving as can be seen from Fig. 8b and d.

The situation in the vicinity of the crack tip in ligament direction is demonstrated in more detail by Fig. 9 **(31)**. Deviating from the basic assumptions of the HRR-theory the crack tip opening displacement and, therefore, the crack

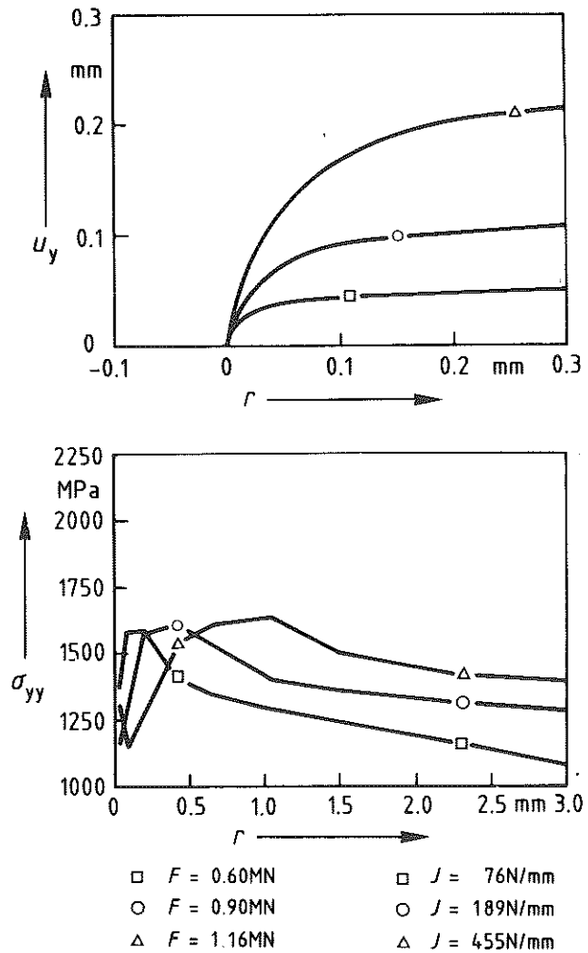

Fig 9 Crack opening displacement COD and crack opening stress σ_{yy} versus distance from crack tip r in a CT 100-specimen at three different levels of J-integral obtained by 2D-FEM (31)
(a) crack tip opening displacement
(b) crack opening stress

tip deformation are not small. In this case the crack opening stress σ_{yy} – plotted as a function of the distance of the crack tip – follows approximately the HRR-field, passes a maximum and decreases considerably, i.e. the HRR-field breaks down in the direct vicinity of the crack tip as has been shown by McMeeking and Parks **(19)**. The maximum of the crack opening stress σ_{yy} is shifted to greater distances from the crack tip with increasing load or J. These distances may be seven times as large as the corresponding crack tip opening displacement. From these findings the conclusion can be drawn that the volume element close to the crack tip with a diameter less than 0.2 mm where fracture initiation takes place is governed by a stress state which is approximately of plane strain but more a biaxial than triaxial one since σ_{xx} becomes small **(32)**.

Figure 10 shows the results from 3D elastic–plastic FE-analysis of CT-specimens of different size **(18)(27)(33)**, demonstrating the influence of thickness and width of CT-specimens on σ_m/σ_v and on ε_v in dependence on the normalising parameter rR_{eL}/J. According to the HRR-theory the ratio σ_m/σ_v should be constant in dependence on r. The numerically calculated curves, however, show a pronounced maximum of σ_m/σ_v – which is lifted with increasing dimensions of the specimen. The most severe influence of size parameters is observed for CT-specimens smaller than CT 100. In contrast to the stresses the equivalent strain increases continuously towards the crack tip. Although the gradient of these curves is not entirely identical with that of the HRR-field **(18)**, the strain concentration adjacent to the crack tip is obvious and increases with decreasing specimen size.

In Fig. 10 the dimensions of the CT-specimen are varied proportional to the thickness as well as to the width parameters. Therefore, in-plane as well as out-of-plane constraint may be influenced simultaneously and the resulting variations of the stress and strain field may be in an indistinguishable manner correlated to both effects. A comparison on the basis of in-plane constraint only is shown in Fig. 11, compiling results of elastic–plastic FE-calculations of CT-, DECT- and CCT-specimens under the simplifying assumption of a plane strain state **(18)**. The maximum in σ_m/σ_v is highest for the CT-specimen followed by that of the double edge cracked tension specimen (DECT) and the centre cracked tension specimen (centre cracked panel) (CCT). This tendency qualitatively may be understood by visualising the kinematics of the deformation process in these specimens **(3)–(5)(11)**. The rather unrestrained slipping developing from the crack tip of a centre cracked panel causes less constraint compared to the crossing lines in front of the crack including a rigid pivot in a CT-specimen. The scatter band in σ_m/σ_v of the CCT-specimen is caused by decreasing stresses during increasing loading. This effect may be attributed to decreasing constraint as a consequence of increasing crack tip opening displacement, although the final reason is not quite clear. Also in this case the equivalent strain ε_v increases continuously towards the crack tip indicating the strain concentration in this area and is not associated with a stress concentra-

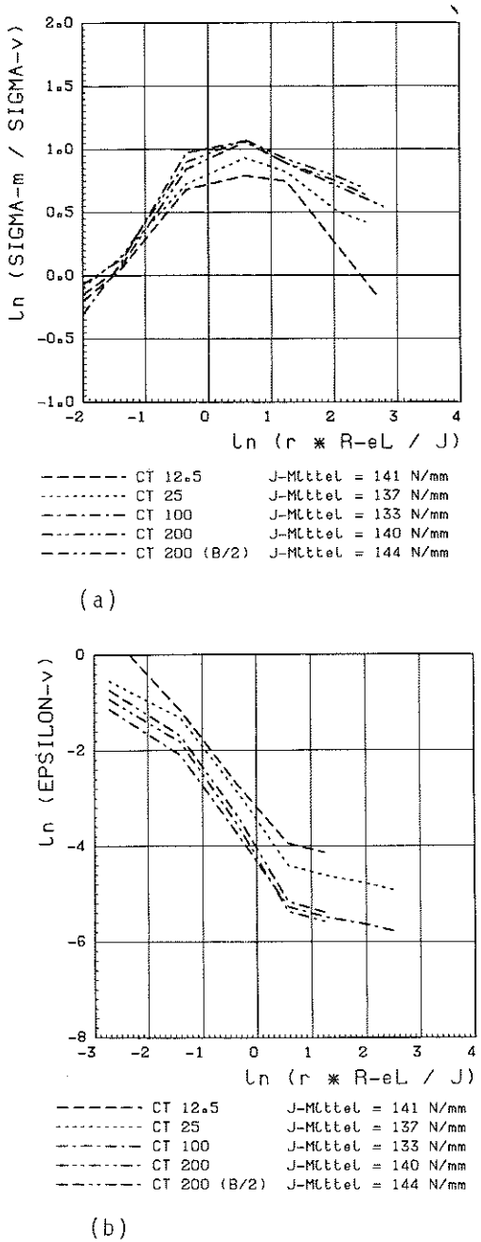

Fig 10 Ratio σ_m/σ_v and equivalent strain ε_v in the mid-plane of CT-specimens of different standard sizes versus normalised ligament rR_{eL}/J obtained by 3D-FEM (18); $\theta = 0°$, $z = 0$
(a) ratio σ_m/σ_v
(b) equivalent strain ε_v

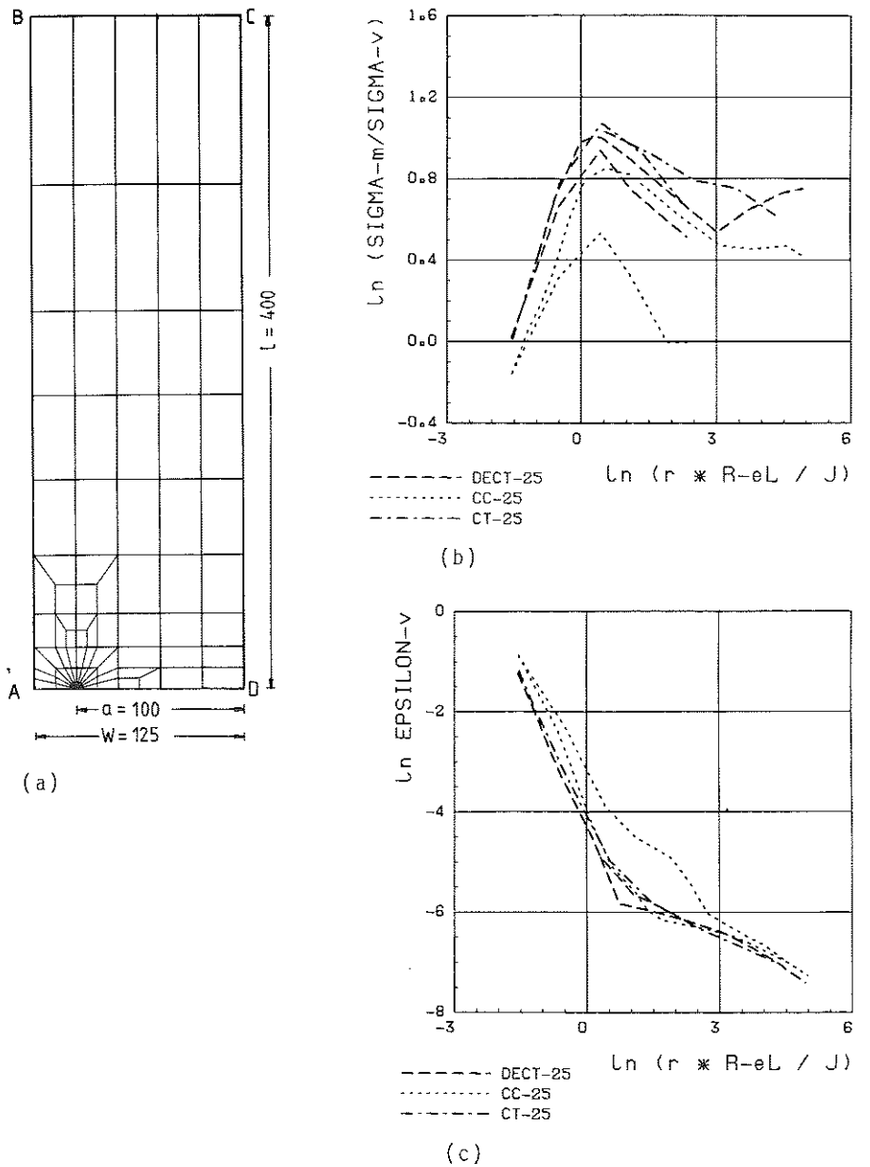

Fig 11 Ratio σ_m/σ_v and equivalent strain ε_v in CT-, DECT-, and CCT-specimen versus normalised ligament rR_{eL}/J obtained by 2D-FEM, plane strain (18); $\theta = 0°$, $J < 164$ N/mm, $r < 4$ mm
(a) geometry of DECT- and CCT-specimen; geometry of CT 25-specimen in accordance with ASTM E 399
(b) ratio σ_m/σ_v
(c) equivalent strain ε_v

tion immediately adjacent to the crack tip. Approaching the crack tip, the differences in terms of stresses and strains between the different types of specimens vanish. Supposed fracture initiation occurs in a volume element of the order of magnitude 0.1–0.2 mm diameter **(26)** there is a strong evidence that different types of specimens do not show any essential difference of initiation values as J_i, although the maximum of the ratio σ_m/σ_v has obviously different levels. In a typical case of a steel with $R_{eL} = 450$ MPa and $J_i = 100$ N/mm the maximum of the ratio σ_m/σ_v is located at about $r = 0.4$ mm. It is interesting to note the crack tip opening displacement-J-correlation follows the same ranking as stresses and strains (Fig. 12). This confirms results of Steenkamp **(34)** considering the proportional factor d_n of equation (1) as a measure of constraint.

As a next step the constraint situation in front of a semi-elliptical internal surface crack in a pressure vessel will be considered. The geometry of the vessel and the crack investigated **(18)(35)** are shown in Fig. 13 together with the variation of the loading parameter J and the maximum of the ratio $\max_x(\sigma_m/\sigma_v)$ along the crack contour given by the parameter Φ. The maximum J is located at the deepest point of the crack as is to be expected for

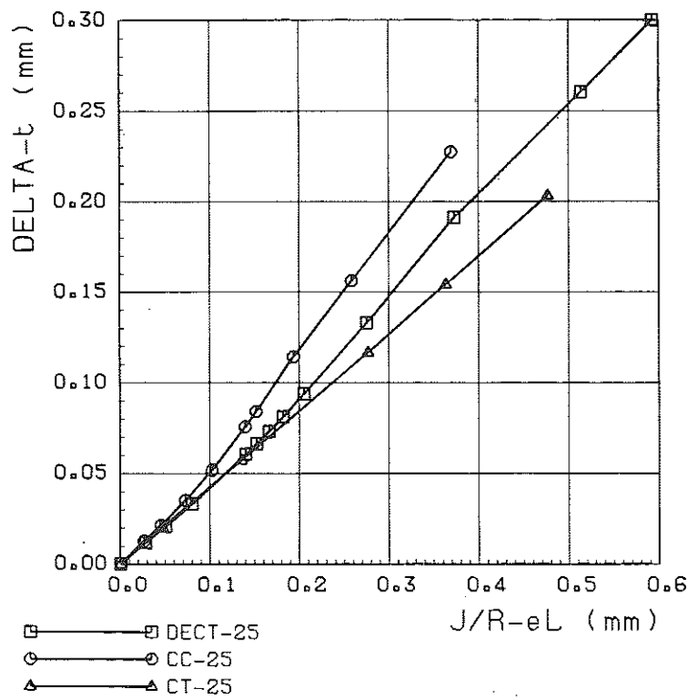

Fig 12 Crack tip opening displacement δ_t in CT-, DECT-, and CCT-specimen versus normalised J-integral J/R_{eL} obtained by 2D-FEM (18), plane strain; specimen geometries like Fig. 11

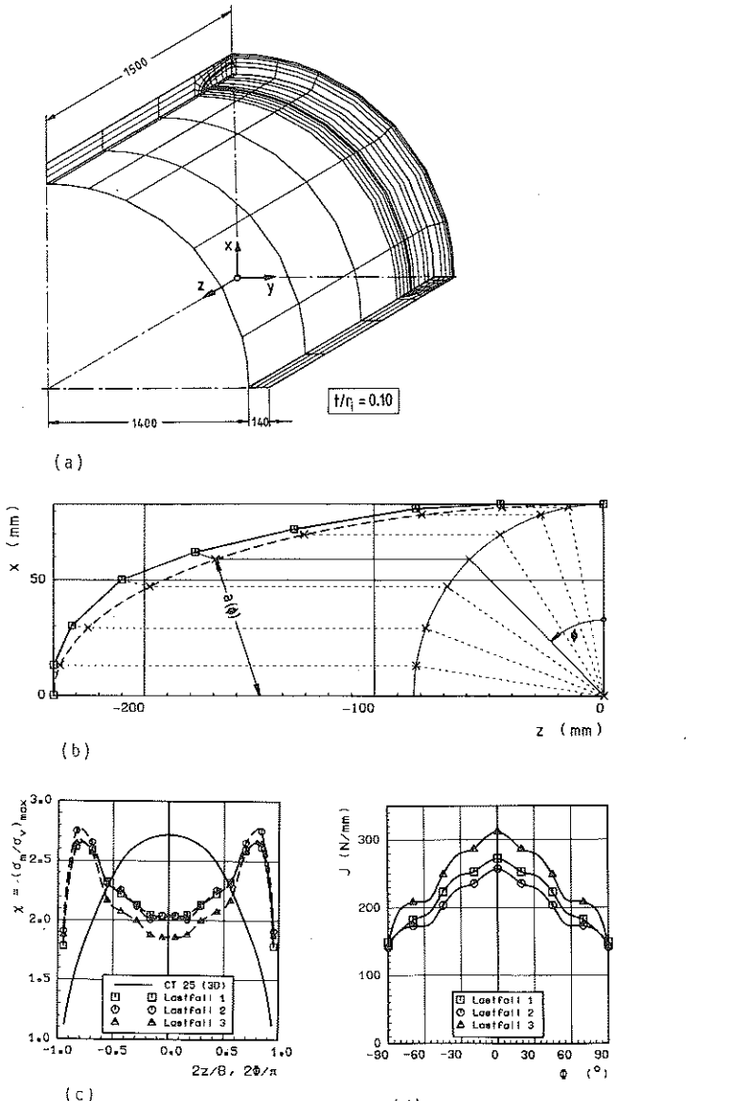

Fig 13 J-integral and maximum value of the ratio σ_m/σ_v at an inner surface crack in a pressure vessel versus the normalised angle Φ obtained by 3D-FEM; loading cases: 1 = internal pressure only, 2 = internal pressure + axial tension (closed vessel), 3 = like 2 + pressure acting on crack surfaces (18)(35)
(a) dimensions of the vessel and view on the whole net structure with 1575 nodes
(b) normalising method in order to obtain Φ
(c) J-integral versus the normalised angle Φ; pressure = 35 MPa
(d) maximum value of the ratio σ_m/σ_v versus the normalised angle Φ; pressure = 35 MPa, comparison with CT-specimen

this configuration. But it is interesting to note that the maximum of constraint in terms of the ratio $\max_{x,\Phi}(\sigma_m/\sigma_v)$ is found at an angle of $\Phi = 75$ degrees and, therefore, does not coincide with the maximum of J.

Local constraint and stable crack growth

The numerical results obtained for non-growing cracks cannot explain the change of gradients of crack resistance curves experimentally observed for different types of specimens as CT- or CCT-specimens. For this purpose further arguments are needed. Supposing that the crack tip resharpens due to the fracture initiation process; this effect consequently will lead to a redistribution of the stress field as well. Figure 14 seems to support these hypothetical considerations **(36)**. These rather new results, not yet confirmed by the same find-

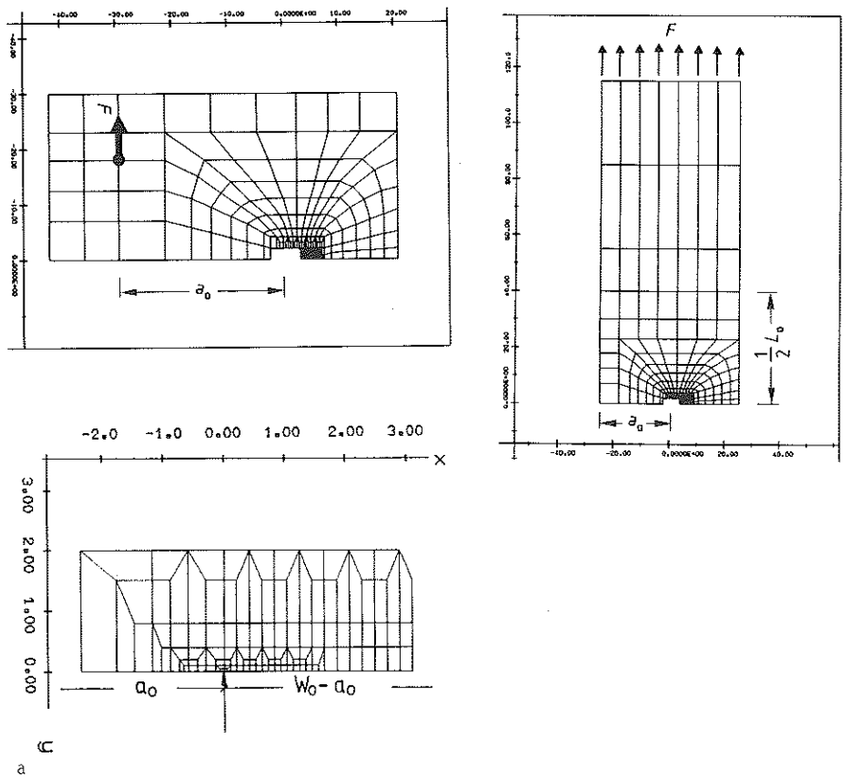

Fig 14 Influence of stable crack growth on the ratio σ_m/σ_v in the vicinity of the crack tip in a CT- and a CCT-specimen (36), material: steel StE 460, R_{eL} = 460 MPa
(a) specimen geometry

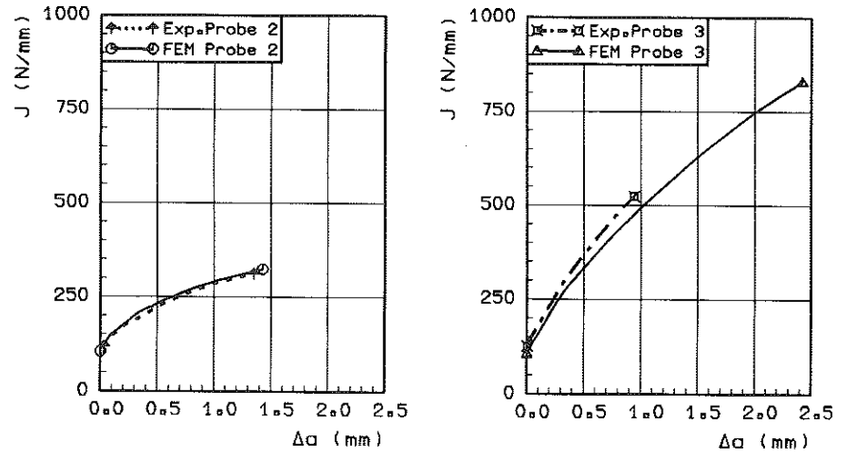

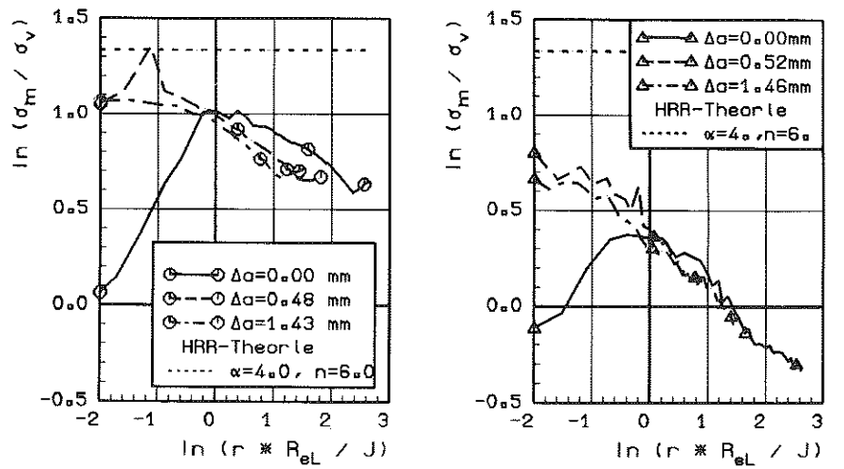

(b) J_R-Δa-curves obtained by experiment and by 2D-FEM (updated Lagrangian formulation, displacement controlled computation)
(c) ratio σ_m/σ_v versus normalised ligament rR_{eL}/J obtained by 2D-FEM

ings of other authors, indicate how the ratio σ_m/σ_v is varying while the crack in a CCT- and in a CT-specimen is growing from $\Delta a = 0$ to 1.4 mm. In both types of specimens for the non-growing cracks $\Delta a = 0$, the same maxima of the ratio σ_m/σ_v as observed in Fig. 11 are found. The level of the maximum of σ_m/σ_v of the CT-specimen does not change very much due to stable crack growth and it is similar to that shown in Fig. 11. Although the geometry of the CCT-specimen as well as the material law (stress-strain-curve) used for the FE-analysis of the growing crack (see Fig. 14) are somewhat different from those used for the FE-analysis of the non-growing crack of Fig. 11, the level of ratio σ_m/σ_v at $\Delta a = 0$ mm in the CCT-specimen in Fig. 14 corresponding to a J-value of 130 N/mm agrees very well with that of the lower bound in Fig. 11 corresponding to a J-value of 85–162 N/mm.

Growing of the crack causes the maximum of σ_m/σ_v to move towards the crack tip. Simultaneously, its level in the CCT-specimen approximately is raised up to the upper bound shown in Fig. 11. The corresponding J-values of the non-growing crack range between 12 to 32 N/mm, but they correspond to very small crack tip opening displacements of less than 0.04 mm. In analogy to Fig. 11 also the maximum of the ratio σ_m/σ_v of the CT-specimen remains approximately unchanged in dependence on crack tip geometry as well as on J even when the crack is growing and is remarkably higher than that of the CCT-specimen. In this context one has to keep in mind that the results of all these FE-calculations with respect to stresses and strains may deviate more or less from reality because the influence of the formation of voids is disregarded by the methodology used.

Summarising these results and disregarding the question of path independence of J for growing cracks **(36)(37)** the influence of the specimen geometry on the gradients of crack resistance curves may be interpreted in the following manner.

- The maxima of the constraint parameter σ_m/σ_v are shifted towards the crack tip due to the resharpening of the growing crack.
- Due to the shift the maxima are located directly in the zone where the fracture process takes place.
- The level of the maximum depends on the specimen geometry and has a pronounced influence on the crack resistance.
- In cases of high local constraint as found in CT-specimens the level of the maxima in σ_m/σ_v observed for the non-growing crack will be maintained while the crack is growing.
- In cases of low constraint as found in CCT-specimens the level of the maximum is raised during crack growth to a value – still lower than that of the previous case – which is correlated to the crack tip opening displacement of the growing crack and which corresponds to the initial value of the maximum of the non-growing crack under low loading. Low loading means in this case $J = 12$ to 32 N/mm.

Micro-mechanical modelling

Based on the work of McClintock **(21)(38)** and of Rice and Tracey **(24)** several authors (e.g. **(22)(23)(39)**) found experimental evidence that the strain to initiate ductile fracture is a function of the ratio σ_m/σ_v. This function is considered as failure locus curve; its shape is characteristic for any material. In order to simulate the ductile failure process, a constitutive equation regarding the influence of the voids on plastic flow must be available. An equation of this kind has been created by Gurson **(40)**. The model of Gurson has been improved by Needleman and Tvergaard **(41)(42)** by taking into account void coalescence. These models provided the basis for the simulation of ductile failure. The aim of these investigations is to establish a correlation between microscopic damage which is characterized by nucleation, growth, and coalescence of voids, and macroscopic material failure including J_R-curves **(25)(26)(44)**.

Experimental evidence of the difference in damage zones is demonstrated in Fig. 15 for tensile bars containing notches with root radii of 4 mm and 0.25 mm. Whereas the local damage for the root radius of 4 mm starts at the centre of the specimen, it occurs close to the notch for the small root radius.

Figure 16 compares the distribution of the void volume fraction of both specimens with that of the ratio σ_m/σ_v. The maxima of the void distribution coincide clearly with those of σ_m/σ_v. The transferability of the damage model has been tested by applying the obtained results to a CT-specimen. For this case the distribution of the volume fraction of voids has been calculated in

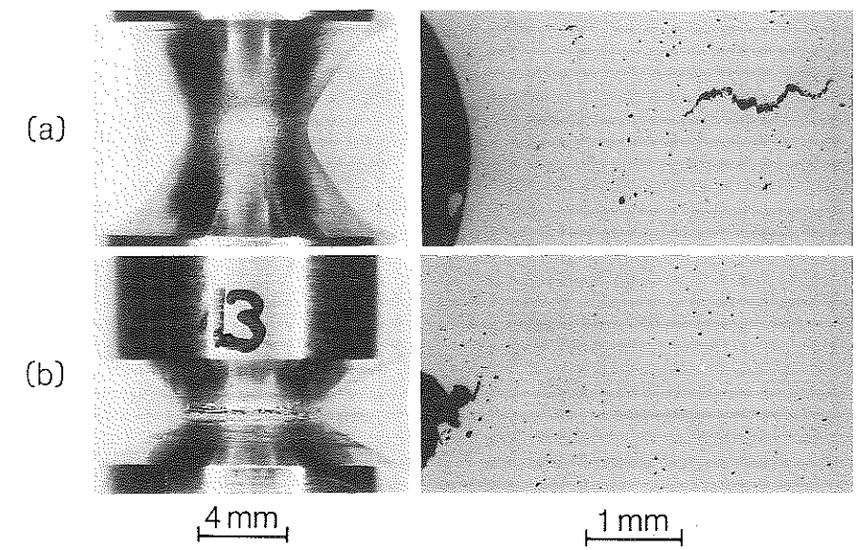

Fig 15 Experimental results on damaging processes during ductile fracture (26); specimen geometries with notch radii of 4.0 and 0.25 mm and micrographs of damage zones

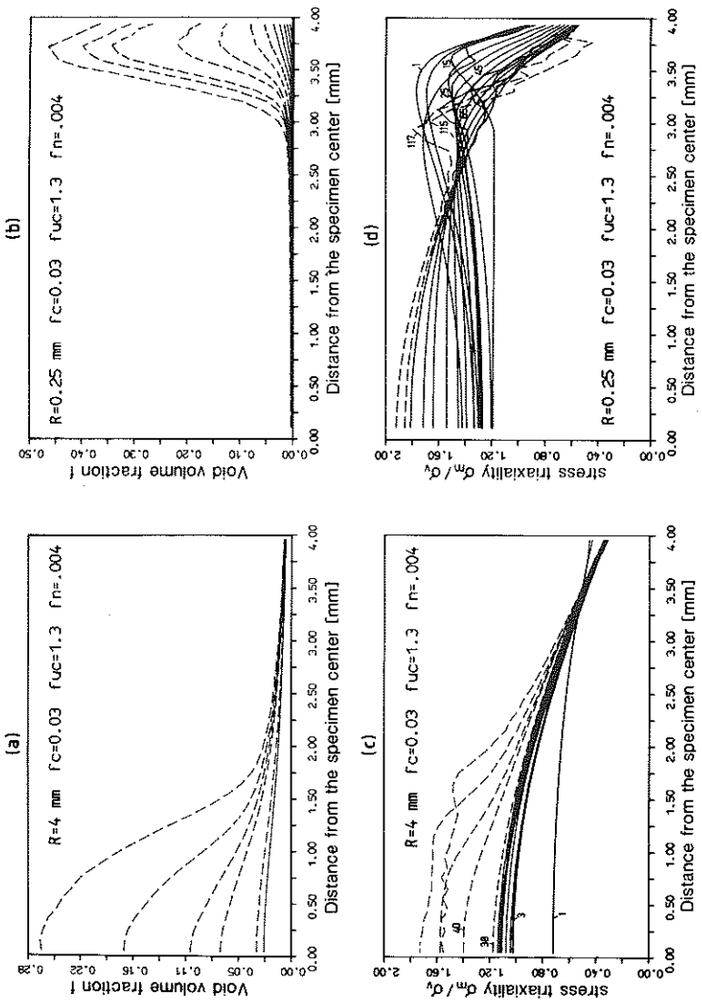

Fig 16 Volume fraction of voids calculated numerically in comparison with the ratio σ_m/σ_v versus distance from mid-axis (26)
(a) volume fraction of voids in the specimen with the notch root radius of 4.0 mm
(b) volume fraction of voids in the specimen with the notch root radius of 0.25 mm
(c) ratio σ_m/σ_v in the specimen with notch root radius of 4.0 mm
(d) ratio σ_m/σ_v in the specimen with notch root radius of 0.25 mm

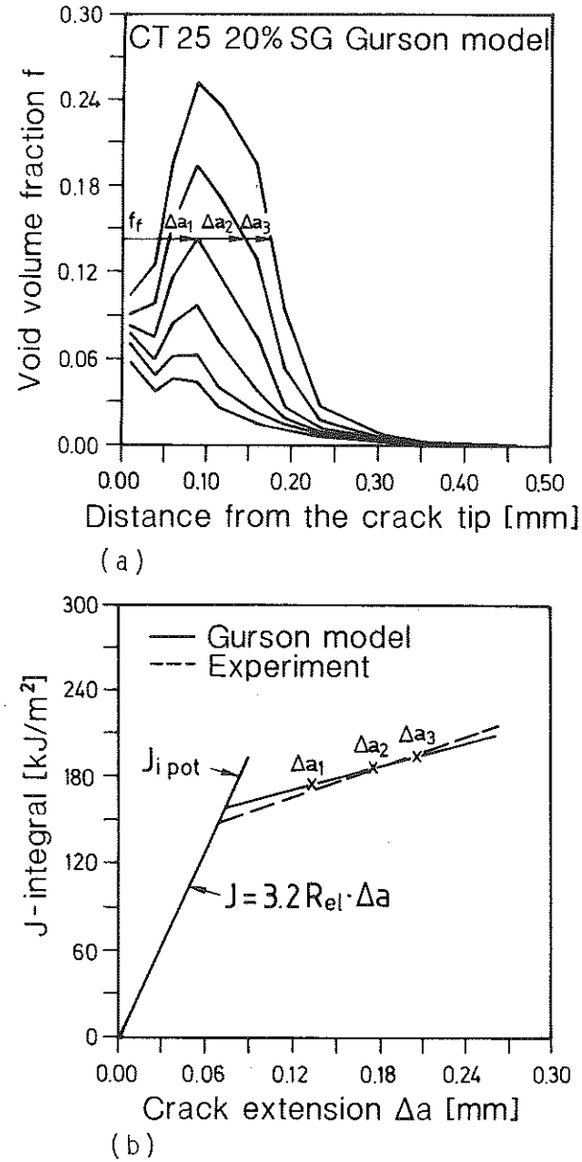

Fig 17 Numerical calculated damaging in a CT 25-specimen, 20 percent sidegrooved, in comparison with experimental results (26)
(a) volume fraction of voids calculated numerically versus distance from the crack tip; the horizontal line indicates the critical value of void volume fraction obtained from notched specimens
(b) calculated crack resistance curve in comparison with the experimentally obtained crack resistance curve

dependence on the distance from the crack tip on the ligament (Fig. 17a). The horizontal line in this figure indicates the critical values of the void volume fraction obtained from the notched tension specimens. Stable crack growth was defined as the size of the damage zone and was calculated for three loading steps. Figure 17b compares the crack resistance curve calculated in this way with that of the corresponding experiment. The accordance is unexpectedly good. This result supports the assumption that the local constraint situation can be expressed by the ratio σ_m/σ_v in a very suitable manner in the case of ductile fracture.

Transferability to components

As a first step in the chain of transferability of results from specimens to components, the extension of surface cracks will be discussed. Investigations of this kind have been carried out by several authors **(27)(28)(45)(46)**.

It is assumed that stable growth of a surface crack can be predicted when the local distribution of the loading parameter J and the resistance parameter J_R as a function of the constraint are known. As an example fracture experiments are considered which are carried out using plates (900 mm × 120 mm × 20 mm) of the steel X 20 CrMoV12 1 at room temperature **(47)**. The original surface crack obtained by fatigue has been extended by stable growth when monotonically increasing load was applied until interruption. The resulting stable crack growth surrounding the contour of the surface crack is shown as a dark zone on the fracture surface in Fig. 18. In order to predict the

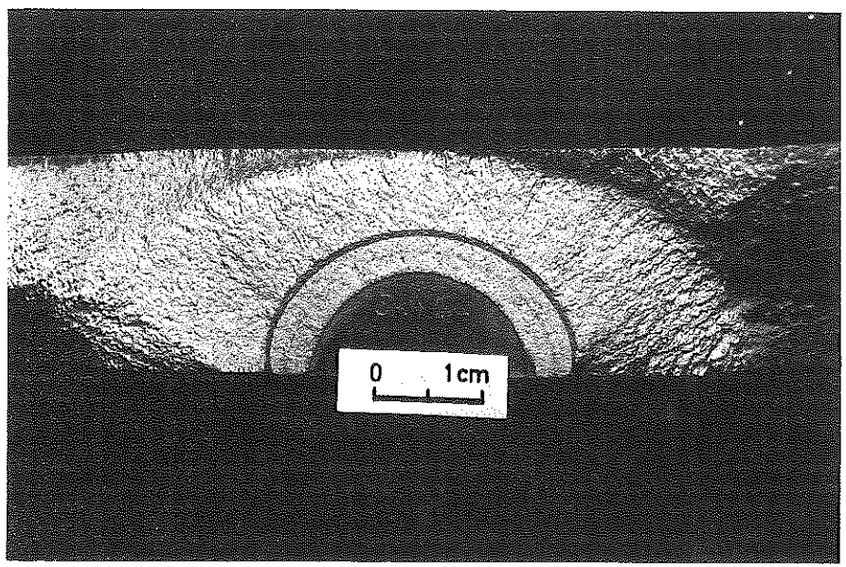

Fig 18 Stable growth of a surface crack in a plate of X 20 CrMoV 12 1 (47)

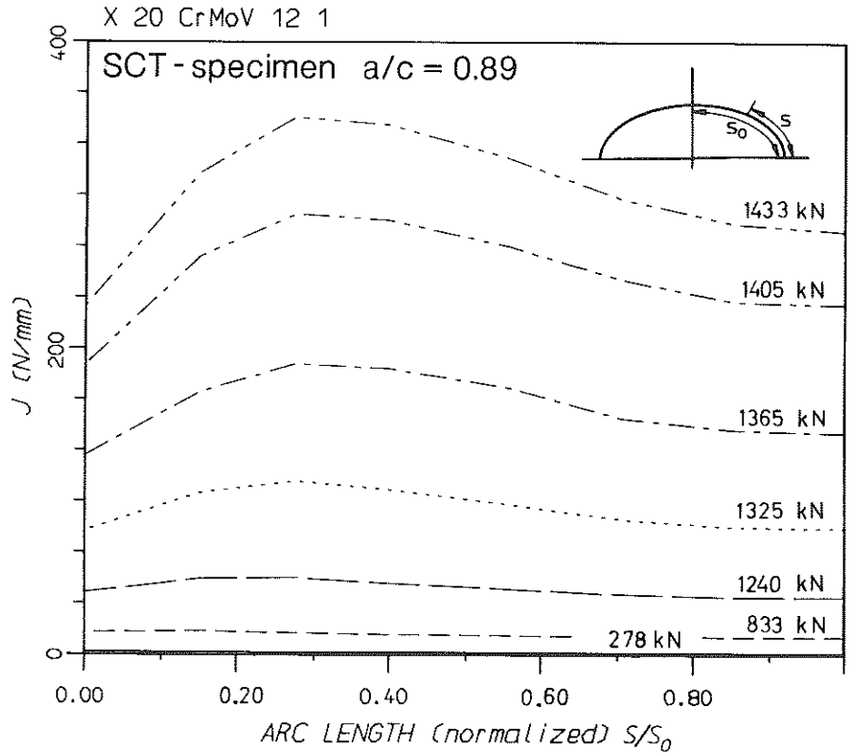

Fig 19 *J*-distribution at several load steps along the contour of a surface crack ($a/c = 0.89$, $a/t = 0.6$) in a plate under remote tension (47)

amount of stable growth in a quantitative manner the following procedure has been applied. The J-distribution at several load steps along the contour of this surface crack, with the dimensions $a/c = 0.89$ and $a/t = 0.6$ in the plate under remote tension, has been computed (Fig. 19) as well as the distribution of $\sigma_m/\sigma_v = \sigma_m/\sigma_v$ ($r = 0.3$ mm, s) on the ligament along the crack contour (Fig. 20). Since the local distribution of the resistance is unknown it can be constructed in the same way as reported in Fig. 21.

In this diagram the $(\Delta J_R/\Delta a)_{mean}$ values experimentally determined from Fig. 2 for the two types of CT-specimens (0 percent sidegrooved: $(\Delta J_R/\Delta a)_{mean} \approx 490$ N/mm^2; 20 percent sidegrooved: $(\Delta J_R/\Delta a)_{mean} \approx 250$ N/mm^2) are plotted versus the corresponding $(\sigma_m/\sigma_v)_{mean}$ calculated at different distances of the crack tip. As a first approximation a linear relationship is assumed and postulated by extrapolation for establishing the slope of resistance curves for cracks in components under different constraint situations. After constructing the

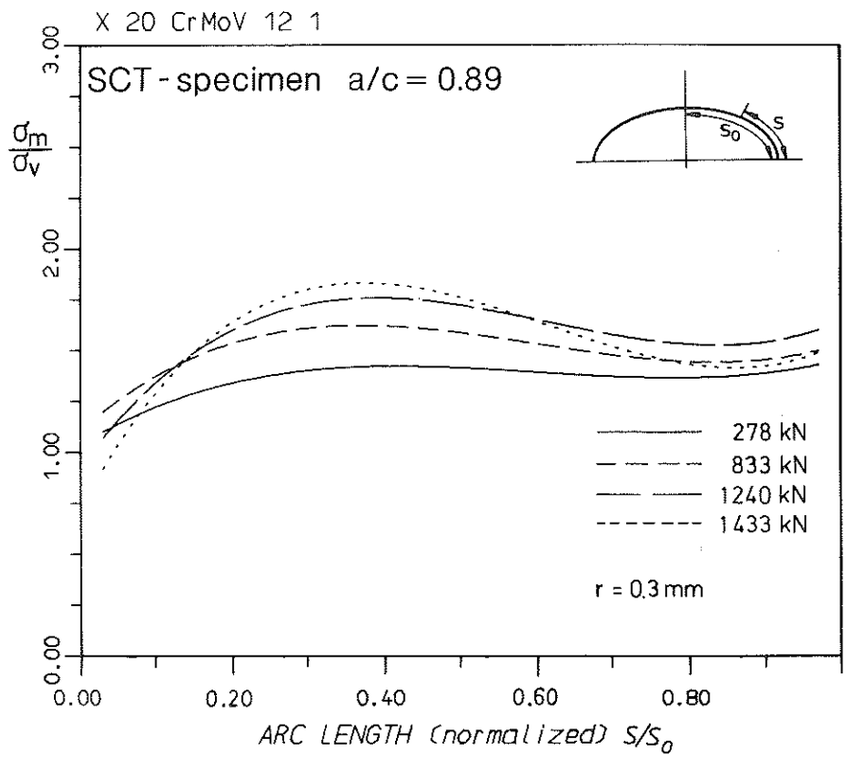

Fig 20 $\sigma_m/\sigma_v = \sigma_m/\sigma_v(s)$ **at the distance** $r = 0.3$ **mm along the contour of the same surface crack** (47)

local resistance curves for the surface crack from its local constraint distribution by means of Fig. 2 and inserting the related local J-values according to Fig. 19, finally the local variation of the crack extension Δa can be estimated. Although this procedure is based on a series of simplifying assumptions, the resulting variation of the local crack extension $\Delta a(s)$ is in excellent agreement with that determined experimentally (Fig. 22).

The following investigations support these findings by taking a similar, but nevertheless different, approach. Tests of a pressure vessel containing an axial outer surface flaw **(16)(17)** are numerically accompanied by elastic–plastic FE-calculations. The results are presented in Fig. 23 in a normalized and condensed form. The surface crack was extended alternately by fatigue and stable crack growth. In order to demonstrate the canoeing effect as clearly as possible. As can be seen from Fig. 23a, the experiment proceeded in four steps. All these steps produced canoeing, the third one in the most pronounced manner. The FE-calculation simulates the first step. J has its maximum at the deepest

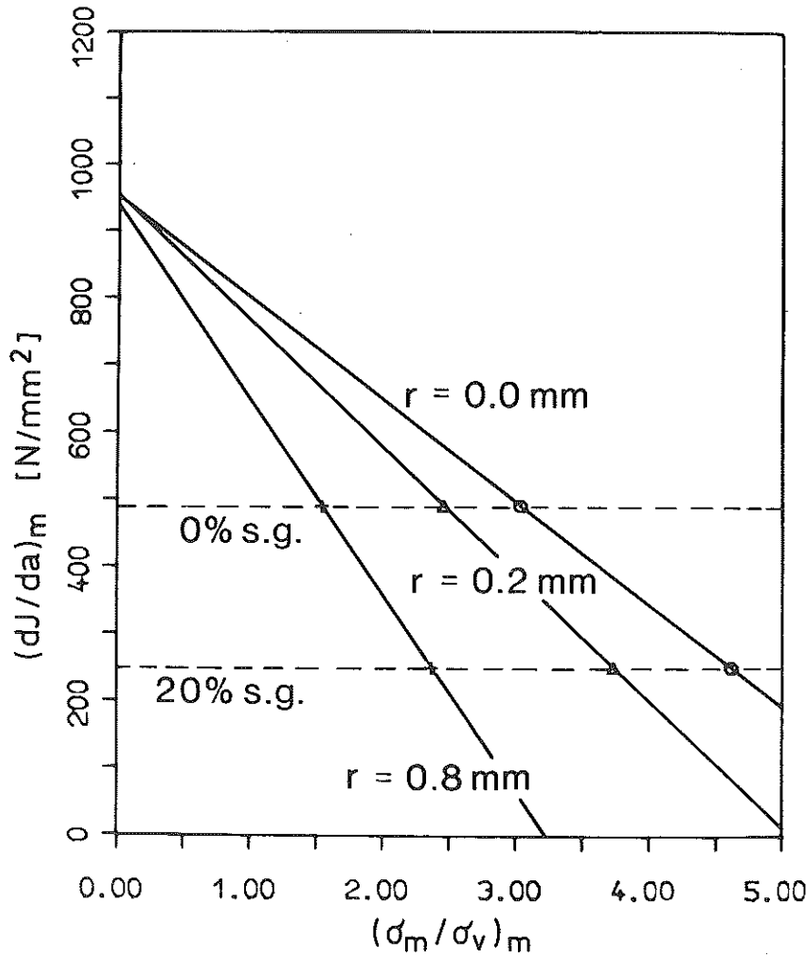

Fig 21 Correlation of slope $(\Delta J_R/\Delta a)_{mean}$ for different crack tip distances r (29)

point of the crack and does not coincide with the maximum of the ratio $\max_{x,\Phi}(\sigma_m/\sigma_v)$. However, the maximum of the ratio $\max_{x,\Phi}(\sigma_m/\sigma_v)$ expressing the local constraint situation, shows coincidence with the maximum of stable crack growth. This demonstrates very clearly that the maximum of stable crack growth does not necessarily occur at maximum of J. This phenomenon can be understood by estimating the crack resistance curves for the different angles Φ **(16)(17)** (Fig. 24). The estimated crack resistance curves in the range of $\Phi = 70$–80 degrees correspond approximately to those of CT-specimens, whereas in the mid-section they may be closer to those of CCT-specimens.

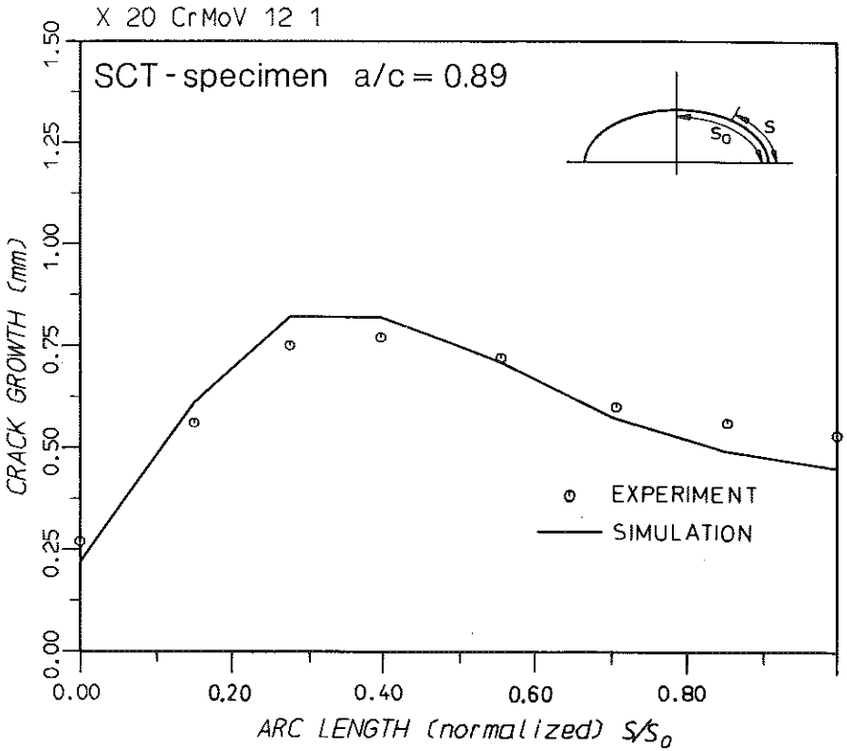

Fig 22 Comparison of the local crack extension constructed and experimentally determined for the same surface crack configuration (47)

Despite higher J-values in the mid-section, the amount of stable crack growth in this section remains lower than that of the range 70–80 degrees because the crack resistance – as a consequence of increasing constraint – decreases more rapidly than J with increasing angle Φ. Therefore, the section next to the surface becomes the area of preferred crack growth (Fig. 23). A further experiment with the steel StE 460 of similar type also accompanied by a FE-calculation has confirmed these results **(17)**.

Conclusions

Based on the assumption that as a first step in the chain of transferability of results from specimens to components the interpretation of the growth behaviour of surface cracks is needed, the following phenomena had to be explained.

- The contours of surface cracks after stable crack growth are not semi-elliptically shaped ('canoeing'-effect) because the maximum of local crack extension is not found in the centre (angle $\Phi = 0$ degrees), but in a range, 60 degrees $< \Phi <$ 80 degrees.
- The maximum amount of stable crack growth does not coincide with the maximum of the loading parameter J numerically calculated along the crack contour.
- The slope of J_R-curves locally constructed at several points along the crack contour differs considerably from that of a resistance curve from a side-

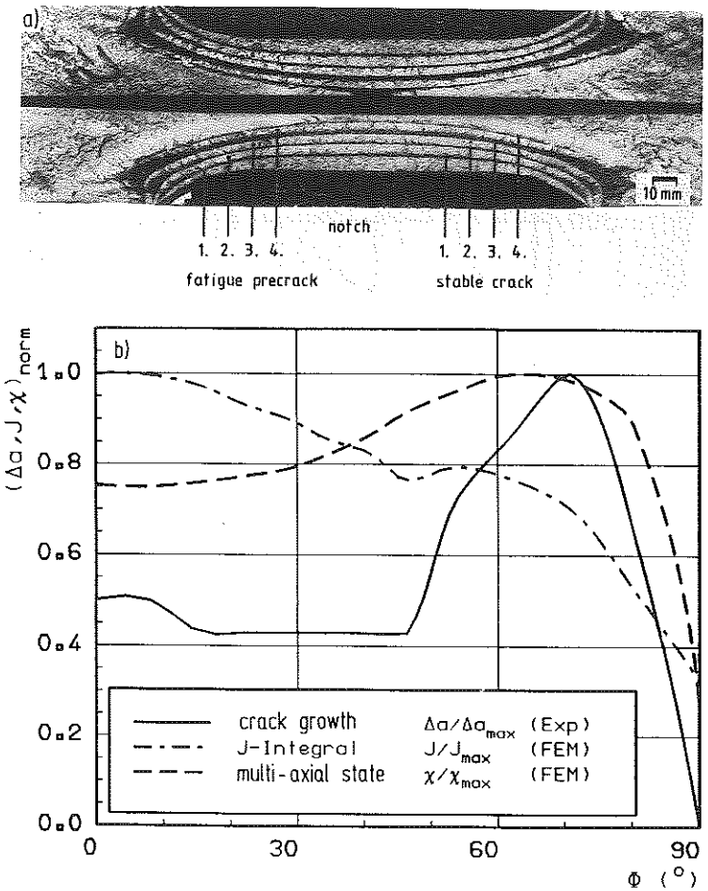

Fig 23 Stable crack growth in pressure vessel with an outer surface crack, comparison of experimental and 3D-FEM results (16); dimensions of the vessel: t = 40 mm, r_i = 750 mm, c_0 = 91 mm, a_0 = 20.5 mm; material: reactor pressure vessel steel 20 MnMoNi 55; $\chi = \sigma_m/\sigma_v$
(a) fracture surfaces
(b) normalized parameter $\chi_{norm} = \max_z (\sigma_m/\sigma_v)/\max_{z,\Phi} (\sigma_m/\sigma_v)$ $J_{norm} = J/J_{max}$, $\Delta a_{norm} = \Delta a/\Delta a_{max}$ obtained by 3D-FEM in comparison with the experimentally obtained amount of stable crack growth (1st step of stable crack growth in Fig. 23a) versus normalised angle Φ

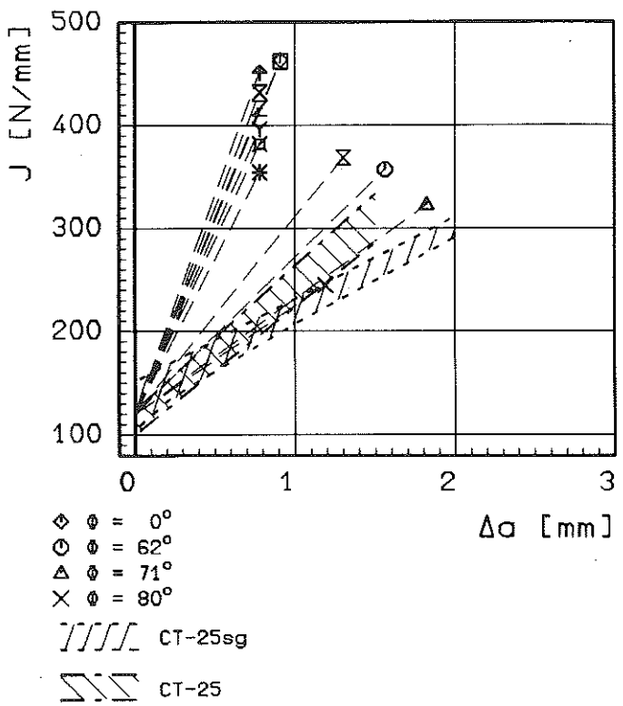

Fig 24 Local crack resistance curves obtained by 3D-FEM and experiment for different angles Φ of the surface flaw shown in Fig. 23a compared with the crack resistance curves of CT-specimens of the same material (16)

grooved CT 25 specimen – except in the range $-60 < \Phi < 80$ degrees – where the maximum crack growth occurs.

For several examples it has been demonstrated that these phenomena can be understood and described when in addition to the local distribution of the loading parameter along the crack contour, such as J, the local constraint situation in terms of the parameter σ_m/σ_v is taken into account and a quantitative relation between the constraint parameter and the governing J_R-curves is established.

The detailed analysis of the constraint behaviour in front of cracks under different geometrical conditions and loading situations leads, furthermore, to the following conclusions:

- The maxima of the constraint parameter σ_m/σ_v are shifted towards the crack tip due to a resharpening when the crack starts to grow.
- Due to this shift for the growing crack the maxima are located directly in the zone where the fracture process takes place.

- The level of the maximum depends on the specimen geometry and has a pronounced influence on the crack resistance.
  - In cases of high local constraint, as found in CT-specimens, the level of the maximum in σ_m/σ_v observed for the non-growing crack will be maintained while the crack is growing;
  - In cases of low constraint as found in CCT–specimens the level of the maximum is raised during crack growth to a value still lower than that of the previous case.

References

(1) SIEBEL, E. and MEYER, A. F. (1933) Z. VDI 77, **51**, 1345–1349.
(2) KRISCH, A. (1935) Spannungsmechanik des gekerbten Rundstabes, *Dr.-Ing.-Diss. Techn. Hochshule*, Berlin.
(3) HILL, R. (1956) The mathematical theory of plasticity, 2nd edn., University Press, Oxford.
(4) GREEN, A. P. (1953) *Quart. J. Mech. and Applied Math.*, **VI**, Pt. 4, 223–239.
(5) GREEN, A. P. and HUNDY, B. B. (1956) *Journ. Mech. Phys. Solids*, **4**, 128–144.
(6) KOCHENDÖRFER, A. and SCHOLL, H. (1957) *Stahl u. Eisen 77*, **15**, 1006–1117.
(7) KOCHENDÖRFER, A. and SCHÜRENKÄMPER, A. (1961) *Arch. Eisenhüttenwes. 32*, **10**, 689–699.
(8) VALTINAT, G. (1971) Kriterium zur Erfassung der Spannungsversprödung von Werkstoffen, *Schriftenreihe Schweißen und Schneiden 2*, **4**, 1–4.
(9) CLAUSMEYER, H. (1969 *Konstruktion 21*, **2**, 52–59.
(10) WITTWER, H.-J. (1975) *Arch. Eisenhüttenwes. 46*, **1**, 41–49.
(11) KNOTT, J. F. (1973) *Fundamentals of fracture mechanics*, Butterworths, London.
(12) ASTM E 813-87 (1987) Determination of J_{Ic}, a measure of fracture toughness, *ASTM Standards*, **10**, American Society for Testing and Materials, Philadelphia.
(13) BLAUEL, J. G. and VOSS, B. (1986) Characterization of Ductile Material Behaviour by J_R-Curves, *ECF 6 Fracture Control of Engineering Structures*, **1**, Amsterdam.
(14) LOSS, F. J., MENKE, B. J., GRAY, R. A., Jr., and HAWTHORNE, J. R. (1979) Curve characterisation of irradiated nuclear pressure vessel steels, Proceedings of US NRC. CSNI Specialists Meeting on Plastic Tearing Instability, St. Louis, MO, September 25–27, Washington University.
(15) AURICH, D., WOBST, K., and KRAFKA, H. (1986) Curves of wide plates and CT25 specimens; comparison of the results of a pressure vessel, 13, *MPA-Seminar, Stuttgart*, MPA, Stuttgart, 46.1–46.20.
(16) BROCKS, W., KRAFKA, H., MÜLLER, W., and WOBST, K. Experimental and numerical investigations of stable crack growth of axial surface flaws in a pressure vessel, to be published in Proceedings of 6th Int. Conf. on Pressure Vessel Technology.
(17) BAM-TECHNISCHER BERICHT ZU DEM VORHABEN (1989) Analyse und Weiterentwicklung bruchmechanischer Versagenskonzepte, Schwerpunkt: Stabiles Rißwachstum und Instabilität, Teilgebiet, *Elastisch–plastische Bruchmechanikanalyse eines Druckbehälters mit axialem Außenoberflächenfehler* (2), BAM: Berlin.
(18) BAM-FORSCHUNGSBERICHT 137 (1987) Analyse und Weiterentwicklung bruchmechanischer Versagenkonzepte auf der Grundlage von Forschungsergebnissen auf dem Gebiet der Komponentensicherheit, *Teilvorhaben: Werkstoffmechanik*, BAM, Berlin.
(19) McMEEKING, R. M. and PARKS, D. M. (1979) On criteria for J-dominance of crack-tip fields in large-scale yielding, in *Elastic–Plastic Fracture, ASTM STP 668*, (Edited by J. D. Landes, J. A. Begley, and G. A. Clarke), pp. 175–194, ASTM: Philadelphia.
(20) BRIDGEMAN, P. W. (1952) *Studies in Large Plastic Flow and Fracture*, McGraw-Hill, New York.
(21) McCLINTOCK, F. A. (1968) *J. Appl. Mechanics*, **35**, 363–371.
(22) HANCOCK, J. W. and MACKENZIE, A. C. (1976) *J. Mech. Phys. Solids*, **24**, 147–169.
(23) HANCOCK, J. W. and COWLING, M. J. (1980) Metal Science, 293–304.
(24) RICE, J. R. and TRACEY, D. M. (1969) *J. Mech. Phys. Solids*, **17**, 201–217.

(25) BETHMONT, M., ROUSSELIER, G., DEVESA, G., and BATISSE, R. (1987) Ductile fracture analysis by means of a local approach, *Transactions of the 9th Intl Conference on Structural Mech. in Reactor Technology*, **G**, (Edited by F. H. Wittman), Fracture Mechanics and NDE, Balkema, Rotterdam, 131–141.
(26) SUN, D.-Z., VOSS, B., and SCHMITT, W. (1988) Numerische und experimentelle Untersuchungen zur Schädigungsentwicklung bei duktilem Bruch, *Vorträge der*, **20**, Sitzung des Arbeitskreises Bruchvorgänge. DVM, Berlin, 479–490.
(27) BROCKS, W., KÜNECKE, G., NOACK, H.-D., and VEITH, H. (1987) On the transferability of fracture mechanics parameters from specimens to structures using FEM, **13**, *MPA-Seminar, Beitrag der Komponenten- und Großenprobenprüfung zur Beurteilung von Bauteilen und Anlagen*, MPA, Stuttgart.
(28) KORDISCH, H. and SOMMER, E. (1986) 3D-effects affecting the precision of lifetime predictions, **19***th Nat. Symposium on Fracture Mechanics*, San Antonio, Texas, 30.1–30.24.
(29) KORDISCH, H., SOMMER, E., and SCHMITT, W. (1987) Einfluß der Mehrachsigkeit auf das stabile Rißwachstum, **13**, *MPA-Seminar*, Stuttgart, 7.1–7.17.
(30) SOMMER, E., KORDISCH, H., and SCHMITT, W. (1988) Interpretation of three dimensional effects in cracked bodies, *Intern. Conf. on Computational Engineering Science*, Atlanta, 8.i.1–8.i.5.
(31) MÜLLER, W. and VEITH, H. (1986) *Int. J. Pres. Ves. Piping*, **26**, 275–294.
(32) CLAUSMEYER, H., KUßMAUL, K., and ROOS, E. (1989) Der Einfluß des Spannungszustandes auf den Versagensablauf angerissener Bauteile aus Stahl, *Mat.-wiss. u. Werkstofftech.*, **20**, 101–117.
(33) KÜNECKE, G., OLSCHEWSKI, J., and ZELEWSKI, M. (1984) FEM-Untersuchungen zum Größeneinfluß bei CT-Proben, *Vorträge der*, **16**, Sitzung des Arbeitskreises Bruchvorgänge, DVM, Berlin, 151–160.
(34) STEENKAMP, P. A. J. M. (1986) Investigation into the validity of *J*-based methods for the prediction of ductile tearing and fracture, *Technische Hochschule*, Delft, Niederlande, Dissertation.
(35) BROCKS, W. (1990) Bruchmechanik druckbeanspruchter Bauteile. (Edited by H. P. Keller) TÜV Rheinland Käln, Carl-Hanser Verlag, München, pp. 261–309.
(36) BARTMANN, S. and BROCKS, W. (1989) Private communication.
(37) BROCKS, W. and YUAN, H. (1989) *Eng. Fract. Mech. 32*, **3**, 459–468.
(38) McCLINTOCK, F. A., KAPLAN, S. M., and BERG, C. A. (1966) *Int. J. Fract. Mech.*, **2**, 614–627.
(39) SUN, D.-Z., HALIM, A., and DAHL, W. (1987) Quantitative Beschreibung des Zusammenhanges zwischen bruchmechanischen Kennwerten und der Mikrostruktur, in *Vorträge der* **19**, Sitzung des Arbeitskreises Bruchvorgänge, DVM, Berlin, 303–313.
(40) GURSON, A. L. (1977) *J. Engng Mat. Tech.*, **99**, 2–15.
(41) NEEDLEMAN, A. and TVERGAARD, V. (1984) *J. Mech. Phys. Sol.*, **32**, 461–490.
(42) NEEDLEMAN, A. and TVERGAARD, V. (1985) *J. Mech. Phys. Sol.*, **35**, 151–183.
(43) SUN, D.-Z., SIEGELE, D., VOSS, B. and SCHMITT, W. (1989) Application of local damage models to the numerical analysis of ductile rupture, *Fatigue, Fract. Engng Mater. Struct.*, **12**, 201–212.
(44) BETHMONT, M., DEVESA, G., ROUSSELIER, G., and SAINTON, L. (1988) Application of local approach of ductile fracture to thermal shock loadings, *Proceedings of the 7th European Conf. on Fracture*, (Edited by E. Czoboly), Budapest, Hungary, (1988) *Failure Analysis – Theory and Practice*, **II**, EMAS: Warley, 933–940.
(45) SOMMER, E. (1989) Progress in the assessment of complex components, *Proceedings ICF* **7**, Houston, 1999–2026.
(46) BROCKS, W. and NOACK, H.-D. (1987) Elastic–plastic FEM analysis of an inner surface flaw in a pressure vessel, *9th Conf. on Structural Mech. in Reactor Technology*, **G**, paper 4/3, Lausanne, 1–7.
(47) KLEMM, W., MEMHARD, D., and SCHMITT, W. (1988) Experimental and numerical investigation of surface cracks in plates and pipes, IAEA Specialists Meeting on Large Scale Testing, Stuttgart.